J|A|C|S
ARTICLES
Published on Web 03/08/2003

Effect of Mutation on Enzyme Motion in Dihydrofolate Reductase

James B. Watney, Pratul K. Agarwal, and Sharon Hammes-Schiffer*

Contribution from the Department of Chemistry, 152 Davey Laboratory, Pennsylvania State University, University Park, Pennsylvania, 16802

Received September 10, 2002; E-mail: shs@chem.psu.edu

Abstract: Hybrid quantum-classical molecular dynamics simulations of a mutant *Escherichia coli* dihydrofolate reductase enzyme are presented. Although residue 121 is on the exterior of the enzyme, experimental studies have shown that the mutation of Gly-121 to valine reduces the rate of hydride transfer by a factor of 163. The simulations indicate that the decrease in the hydride transfer rate for the G121V mutant is due to an increase in the free energy barrier. The calculated free energy barrier is higher for the mutant than for the wild-type enzyme by an amount that is consistent with the experimentally observed rate reduction. The calculated transmission coefficients are comparable for the wild-type and mutant enzymes. The simulations suggest that this mutation may interrupt a network of coupled promoting motions proposed to play an important role in DHFR catalysis. This phenomenon has broad implications for protein engineering and drug design.

I. Introduction

Dihydrofolate reductase (DHFR) is vital to normal folate metabolism in prokaryotes and eukaryotes. It catalyzes the reduction of 7,8-dihydrofolate (DHF) to 5,6,7,8-tetrahydrofolate (THF) using nicotinamide adenine dinucleotide phosphate (NADPH) as a coenzyme.[1] In this reaction, the pro-*R* hydride of NADPH is transferred to the C6 of the pterin substrate with concurrent protonation at the N5 position. Because THF is essential for the biosynthesis of purines, pyrimidines, and amino acids, DHFR has been favored as a pharmacological target. As a result of its biological importance, DHFR has been studied extensively with a wide range of experimental and theoretical methodologies.

Previous studies have provided evidence of the importance of enzyme motion in DHFR. X-ray crystallographic structures indicate that the *Escherichia coli* DHFR enzyme assumes different conformations along the reaction pathway.[2] In particular, depending on the nature of the bound ligand, three different conformations have been observed for a surface loop formed by residues 9−24 (denoted the Met-20 loop). When the DHFR substrate and NADPH coenzyme are bound, the Met-20 loop adopts the closed conformation, which is stabilized by hydrogen bonding interactions between the Met-20 loop and the βF−βG loop (residues 117−131). NMR relaxation experiments indicate that the binding of the substrate and coenzyme alters the motion of the enzyme in regions far from the binding sites, including the Met-20 and βF−βG loops, as well as in the active site.[3,4] Classical molecular dynamics simulations identified correlated and anticorrelated side-chain motions in spatially separated regions (including the Met-20 and βF−βG loops) when DHF is bound but not when THF is bound.[5] All of these data suggest a catalytic role for conformational changes in DHFR.

Recently, a network of coupled promoting motions was proposed to play an important role in DHFR catalysis.[6,7] Evidence for this network was obtained by a combination of genomic analysis, kinetic measurements on multiple mutations, and hybrid quantum-classical molecular dynamics. Figure 1 depicts the conserved regions across 36 species of DHFR from *E. coli* to human. Many of the conserved residues are in the active site and therefore impact the binding of the substrate and coenzyme. Several conserved residues, however, are far from the active site, including residues 121−123, which are contained in the βF−βG loop. Although these distal residues may be conserved for structural purposes, they might also be conserved to preserve a network of motions. Kinetic measurements indicate that double mutations involving Gly-121 and Met-42, which are conserved residues distal to the active site and separated by ∼19 Å, are nonadditive (i.e., the effect of a double mutation is greater than the sum of the effects of the single mutations[8]). This nonadditivity suggests a coupling of the βF−βG loop to distant regions of the enzyme, although these kinetic measurements do not distinguish between structural and dynamical effects.

(1) Miller, G. P.; Benkovic, S. J. *Chem. Biol.* **1998**, *5*, R105−R113.
(2) Sawaya, M. R.; Kraut, J. *Biochemistry* **1997**, *36*, 586−603.
(3) Falzone, C. J.; Wright, P. E.; Benkovic, S. J. *Biochemistry* **1994**, *33*, 439−442.
(4) Osborne, M. J.; Schnell, J.; Benkovic, S. J.; Dyson, H. J.; Wright, P. E. *Biochemistry* **2001**, *40*, 9846−9859.
(5) Radkiewicz, J. L.; Brooks, C. L. *J. Am. Chem. Soc.* **2000**, *122*, 225−231.
(6) Agarwal, P. K.; Billeter, S. R.; Rajagopalan, P. T. R.; Benkovic, S. J.; Hammes-Schiffer, S. *Proc. Natl. Acad. Sci.* **2002**, *99*, 2794−2799.
(7) Agarwal, P. K.; Billeter, S. R.; Hammes-Schiffer, S. *J. Phys. Chem. B* **2002**, *106*, 3283−3293.
(8) Mildvan, A. S.; Weber, D. J.; Kuliopulos, A. *Arch. Biochem. Biophys.* **1992**, *294*, 327−340.

10.1021/ja028487u CCC: $25.00

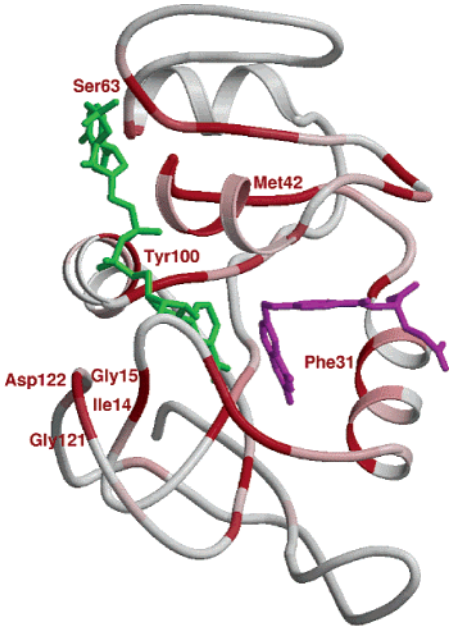

Figure 1. Three-dimensional structure of *E. coli* DHFR. As in ref 6, the residues conserved across numerous species from *E. coli* to human are indicated by a gradient color scheme (grey to red, where red is the most conserved). NADPH and DHF are in green and magenta, respectively. Reproduced with permission from ref 6.

Hybrid quantum-classical molecular dynamics simulations[9] have provided further information about this network of coupled promoting motions. In this approach, the overall rate is expressed as the product of an equilibrium transition state theory rate, which is directly related to the activation free energy barrier, and a transmission coefficient, which accounts for dynamical recrossings of the barrier. The electronic quantum effects are included with a two-state empirical valence bond (EVB) potential,[10] and the nuclear quantum effects are included by representing the transferring hydrogen nucleus as a three-dimensional vibrational wave function. The free energy profile is calculated as a function of a collective reaction coordinate comprised of motions from the entire solvated enzyme. The transmission coefficient is calculated with a reactive flux scheme in which an ensemble of real-time dynamical trajectories is initiated at the top of the barrier and propagated backward and forward in time. This hybrid approach allows us to distinguish between thermally averaged motions that influence the activation free energy barrier and dynamical motions that influence the barrier recrossings. Because the activation free energy barrier is in the exponential of the rate expression, whereas the transmission coefficient is a prefactor of this exponential, the motions influencing the activation free energy barrier are expected to have a greater impact on the enzymatic activity than the motions influencing the barrier recrossings.

Previously we have defined the term "promoting motions" as systematic changes in thermally averaged equilibrium properties along the collective reaction coordinate (i.e., as the reaction evolves from the reactant to the transition state to the product).[6,11,12] Note that this definition does not differentiate between motions playing an active role in catalysis and motions responding to alterations caused by catalysis. Moreover, promoting motions are fundamentally different from promoting vibrations or promoting modes,[13,14] which typically occur on a subpicosecond time scale. Promoting motions are averaged over these fast vibrations of the enzyme and occur on the much longer time scale of the catalyzed chemical reaction. These promoting motions reflect the conformational changes that occur during the chemical reaction. They contribute to the collective reaction coordinate and influence the activation free energy barrier. In the case of DHFR, we have identified and characterized a network of coupled promoting motions extending throughout the enzyme.[6,7]

In this paper, we use hybrid quantum-classical molecular dynamics to investigate the G121V mutant DHFR. Experimental studies have shown that the mutation of Gly-121 to valine reduces the rate of hydride transfer by a factor of 163.[15,16] Residue 121 is on the exterior of the enzyme in the βF$-\beta$G loop, more than 12 Å from the transferring hydride. The goal of our hybrid quantum-classical molecular dynamics simulations is to elucidate this dramatic rate reduction upon mutation of a distal residue. This investigation involves several different types of analyses. First, the structural differences between the wild-type and mutant DHFR are illustrated. Second, the coupled promoting motions (i.e., thermally averaged conformational changes along the collective reaction coordinate) are compared for the wild-type and mutant DHFR. Third, the calculated transmission coefficients, which account for dynamical recrossings of the free energy barrier, are compared. The results suggest that mutation of Gly-121 to valine in *E. coli* DHFR may interrupt the network of coupled promoting motions proposed to play an important role in DHFR catalysis.

II. Theory and Methods

The system used in our DHFR calculations contains the solvated protein, an NADPH cofactor, and a protonated DHFR substrate in a truncated octahedral periodic box. The initial coordinates for the wild-type simulations were obtained from a crystal structure of *E. coli* DHFR complexed with $NADPH^+$ and folate (PDB code 1rx2).[2] In this crystal structure, the Met20 loop is in the closed configuration, which is thought to be the active form for the hydride transfer reaction. The reaction studied is the transfer of the pro-*R* hydrogen on the donor carbon of NADPH to the acceptor carbon of the protonated DHF. The mechanism of this enzyme reaction has been studied previously with ab initio, quantum mechanical/molecular mechanical, and free energy perturbation methods.[17−19] Because a crystal structure of the G121V mutant is not available at this time, we mutated Gly-121 to valine from the crystal structure of the wild-type DHFR. The SwissPDB viewer's rotamer library was used to determine the most stable rotamer.[20]

The electronic ground state potential energy surface is determined with a two-state empirical valence bond (EVB)

(9) Billeter, S. R.; Webb, S. P.; Iordanov, T.; Agarwal, P. K.; Hammes-Schiffer, S. *J. Chem. Phys.* **2001**, *114*, 6925−6936.
(10) Warshel, A. *Computer Modeling of Chemical Reactions in Enzymes and Solutions*; John Wiley & Sons: New York, 1991.
(11) Billeter, S. R.; Webb, S. P.; Agarwal, P. K.; Iordanov, T.; Hammes-Schiffer, S. *J. Am. Chem. Soc.* **2001**, *123*, 11 262−11 272.
(12) Hammes-Schiffer, S. *Biochemistry* **2002**, *41*, 13 335−13 343.
(13) Antoniou, D.; Schwartz, S. D. *J. Phys. Chem. B* **2001**, *105*, 5553−5558.
(14) Cui, Q.; Karplus, M. *J. Phys. Chem. B* **2002**, *106*, 7927−7947.
(15) Cameron, C. E.; Benkovic, S. J. *Biochemistry* **1997**, *36*, 15 792−15 800.
(16) Rajagopalan, P. T. R.; Lutz, S.; Benkovic, S. J. *Biochemistry* **2002**, *41*, 12 618−12 628.
(17) Cummins, P. L.; Gready, J. E. *J. Comput. Chem.* **1998**, *19*, 977.
(18) Cummins, P. L.; Gready, J. E. *J. Am. Chem. Soc.* **2001**, *123*, 3418−3428.
(19) Castillo, R.; Andres, J.; Moliner, V. *J. Am. Chem. Soc.* **1999**, *121*, 12 140−12 147.
(20) Guex, N.; Peitsch, M. C. *Electrophoresis* **1997**, *18*, 2714.

potential.[10] In VB state 1, the hydride is bonded to its donor carbon, whereas in VB state 2, the hydride is bonded to its acceptor carbon. The diagonal elements of the 2 × 2 EVB Hamiltonian are described by the GROMOS force field 43A1[21,22] with modifications described in ref 7. These modifications include the use of a Morse potential for the bond between the transferring hydride and the donor or acceptor. The coupling between the two VB states (i.e., the off-diagonal matrix element) is assumed to be a constant V_{12}, and a constant energy adjustment Δ_{12} is added to the energy of the second VB state. The parameters V_{12} and Δ_{12} were chosen to ensure that the quantum free energy profile for the reaction reproduces the experimentally determined maximal forward and reverse rates for hydride transfer in wild-type DHFR.[23] The values determined for these parameters are $V_{12} = 29.95$ kcal/mol and $\Delta_{12} = 59.87$ kcal/mol. (Note that these have been slightly refined since the simulations in ref 7.) The same EVB parameters were used for the mutant studies except for the replacement of Gly-121 with valine.

The free energy profiles are calculated as functions of a collective reaction coordinate analogous to the solvent coordinate used in Marcus theory for electron transfer.[24−26] The nuclear quantum effects[27,28] are included by representing the transferring hydrogen nucleus as a three-dimensional vibrational wave function.[29,30] Within this framework, the collective reaction coordinate is defined as the difference between the energies of the two VB states averaged over the lowest energy hydrogen vibrational wave function

$$\Lambda(\mathbf{R}) = \langle \Phi_0(\mathbf{r};\mathbf{R}) | V_{11}(\mathbf{r},\mathbf{R}) - V_{22}(\mathbf{r},\mathbf{R}) | \Phi_0(\mathbf{r};\mathbf{R}) \rangle \quad (1)$$

where **r** represents the coordinate of the transferring hydrogen nucleus and **R** represents the coordinates of the remaining nuclei. $V_{11}(\mathbf{r},\mathbf{R})$ and $V_{22}(\mathbf{r},\mathbf{R})$ are the energies of VB states 1 and 2, respectively, and $\Phi_0(\mathbf{r};\mathbf{R})$ represents the ground state hydrogen vibrational wave function. This reaction coordinate is physically meaningful for a two-state charge transfer reaction in which one state is lower in energy for the reactant and the other state is lower in energy for the product. Moreover, this choice of reaction coordinate has been shown to be reasonable for these types of systems because the calculated transmission coefficient (i.e., recrossing factor) is near unity.[7,11]

A series of mapping potentials is used to sample the relevant range of the collective reaction coordinate. These mapping potentials[10] are defined to be linear combinations of the energies of the two VB states

$$V_{\text{map}}(\mathbf{r},\mathbf{R};\lambda) = (1-\lambda)V_{11}(\mathbf{r},\mathbf{R}) + \lambda V_{22}(\mathbf{r},\mathbf{R}) \quad (2)$$

As the mapping parameter λ is varied from zero to unity, the reaction progresses from the reactant VB state 1 to the product VB state 2. Individual pieces of the free energy profile are calculated with different mapping potentials and are connected using thermodynamic integration. This allows us to generate the entire adiabatic quantum free energy profile along the reaction coordinate. The free energy barrier $\Delta G^{\dagger}$ obtained from these free energy profiles is used to calculate a transition state theory rate constant from the expression[31]

$$k_{\text{TST}} = \frac{k_{\text{B}}T}{h} e^{-\Delta G^{\dagger}/k_{\text{B}}T} \quad (3)$$

where k_{B} is Boltzmann's constant.

The equilibration procedure for the generation of the free energy profiles was similar to that described in ref 7. The integration step was 1 fs for these simulations. The initial equilibration involved four steps, each consisting of a geometry optimization followed by 5 ps molecular dynamics, gradually releasing the force constant of position restraints to the crystal structure positions from 100 kcal/(mol Å^2) to 50, 25, and 0 kcal/(mol Å^2). After an additional 20 ps molecular dynamics, the free energy profiles were generated through a series of 11 different mapping potentials. For each mapping potential, the final coordinates from the previous mapping parameter were first optimized, and then the system was equilibrated for 5 ps. The configurations were then equilibrated for another 100 ps, followed by 200 ps of data collection for each mapping potential.

The transmission coefficient is calculated by combining the reactive flux scheme for infrequent events[32−36] with a surface hopping method[37,38] to include vibrationally nonadiabatic effects. The transmission coefficient κ accounts for the dynamical recrossings of the dividing surface and is defined by the expression

$$k_{\text{dyn}} = \kappa k_{\text{TST}} \quad (4)$$

where k_{dyn} is the exact rate constant. In the reactive flux approach, κ is calculated as the flux-weighted average of a quantity ξ for a canonical ensemble of molecular dynamics trajectories started at the dividing surface and integrated backward and forward in time. The quantity ξ corrects for multiple crossings of the dividing surface and is defined to be $1/\alpha$ for trajectories that have α forward crossings and α-1 backward crossings of the dividing surface and zero otherwise.

The fundamental principle of the MDQT surface hopping method[37,38] is that an ensemble of trajectories is propagated, and each trajectory moves classically on a single adiabatic vibrational surface except for instantaneous transitions among the adiabatic vibrational states. These transitions are incorporated with Tully's fewest switches algorithm, which apportions

(21) van Gunsteren, W. F.; Billeter, S. R.; Eising, A. A.; Hunenberger, P. H.; Kruger, P.; Mark, A. E.; Scott, W. R. P.; Tironi, I. G. *Biomolecular Simulation*: *The GROMOS96 Manual and User Guide*; VdF Hochschulverlag: ETH Zurich: Zurich, 1996.
(22) Scott, W. R. P.; Hunenberger, P. H.; Tironi, I. G.; Mark, A. E.; Billeter, S. R.; Fennen, J.; Torda, A. E.; Huber, T.; Kruger, P.; van Gunsteren, W. F. *J. Phys. Chem. A* **1999**, *103*, 3596−3607.
(23) Fierke, C. A.; Johnson, K. A.; Benkovic, S. J. *Biochemistry* **1987**, *26*, 4085−4092.
(24) Marcus, R. A. *Ann. Rev. Phys. Chem.* **1964**, *15*, 155−196.
(25) Warshel, A. *J. Phys. Chem.* **1982**, *86*, 2218.
(26) King, G.; Warshel, A. *J. Chem. Phys.* **1990**, *93*, 8682−8692.
(27) Staib, A.; Borgis, D.; Hynes, J. T. *J. Chem. Phys.* **1995**, *102*, 2487−2505.
(28) Laria, D.; Ciccotti, G.; Ferrario, M.; Kapral, R. *J. Chem. Phys.* **1992**, *97*, 378−388.
(29) Webb, S. P.; Hammes-Schiffer, S. *J. Chem. Phys.* **2000**, *113*, 5214−5227.
(30) Iordanov, T.; Billeter, S. R.; Webb, S. P.; Hammes-Schiffer, S. *Chem. Phys. Lett.* **2001**, *338*, 389−397.
(31) Wigner, E. *J. Chem. Phys.* **1937**, *5*, 720−725.
(32) Neria, E.; Karplus, M. *J. Chem. Phys.* **1996**, *105*, 10 812−10 818.
(33) Bennett, C. H. *Algorithms for Chemical Computation*; American Chemical Society: Washington, DC, 1997.
(34) Keck, J. C. *J. Chem. Phys.* **1960**, *32*, 1035−1050.
(35) Anderson, J. B. *J. Chem. Phys.* **1973**, *58*, 4684−4692.
(36) Chandler, D. In *Classical and Quantum Dynamics in Condensed Phase Simulations*; Berne, B. J., Ciccotti, G., Coker, D. F., Eds.; World Scientific: Singapore, 1998; pp 3−23.
(37) Tully, J. C. *J. Chem. Phys.* **1990**, *93*, 1061−1071.
(38) Hammes-Schiffer, S.; Tully, J. C. *J. Chem. Phys.* **1994**, *101*, 4657−4667.

trajectories among the adiabatic vibrational states according to the quantum probabilities, as determined by integration of the time-dependent Schrödinger equation. The combination of the reactive flux and MDQT methods is complicated by the dependence of the quantum amplitudes on the history of the trajectory. These difficulties are surmounted by implementation of the method presented in ref 39.

In our reactive flux calculations, the dividing surface was chosen to be $\Lambda = 0$ kcal/mol. The initial conditions for the trajectories at the dividing surface were chosen to be the 95 configurations closest to the dividing surface obtained from the equilibrium simulations for the mapping potential with $\lambda = 0.5$. In each case, four different sets of Boltzmann-distributed velocities were used for each coordinate configuration. All trajectories were initiated in the vibrational ground state at the dividing surface since the higher states were shown previously to be negligible.[7] The time step for these MDQT calculations was 0.5 fs.

III. Results

We calculated the adiabatic quantum free energy profile as a function of the collective reaction coordinate for wild-type and mutant DHFR. The calculated free energy barrier was 3.4 kcal/mol higher for the G121V mutant than for the wild-type DHFR. This result is qualitatively consistent with the experimental observation[15,16] of a rate reduction by a factor of 163, corresponding to an increase in the free energy barrier of 3.0 kcal/mol. Note that the experimental activation free energy barriers for the wild-type and mutant enzymes were determined by neglecting dynamical barrier recrossings, i.e., by assuming a transmission coefficient of unity. As shown below, this is a reasonable approximation based on the calculated transmission coefficients.

These equilibrium simulations also provide information about the structural differences between wild-type and mutant DHFR for the reactant and transition state. Figure 2 illustrates the differences among these structures, and Table 1 compares selected average geometrical properties. The average structures were obtained from the 100 configurations closest to the reactant minimum of the free energy profile ($\Lambda = -161$ and -169 kcal/mol for wild-type and mutant DHFR, respectively) and from the 95 configurations closest to the transition state ($\Lambda = 0$ kcal/mol). For each case, the structures were aligned by minimizing the root-mean-square deviation of the alpha carbon atoms, and the Cartesian coordinates were averaged with the appropriate statistical weightings used to generate the free energy profiles. Figure 2 illustrates that the wild-type and mutant DHFR averaged structures are very similar. The main structural differences are found in the loop regions (i.e., the Met-20 and βF-βG). This observation is consistent with NMR experiments showing these loops to be highly mobile.[3,4]

We also performed a more detailed analysis in the region near the mutation. The equivalent of *E. coli* residue 121 is conserved as glycine in prokaryotes and is typically serine or cysteine in eukaryotes.[6] Often, the equivalent of *E. coli* residue 13 is valine in prokaryotes and glycine in eukaryotes, suggesting possible steric constraints in this region. Figure 3 depicts residue 121 in the βF$-\beta$G loop and Val-13 in the Met-20 loop for the wild-type and mutant DHFR average structures. Even though

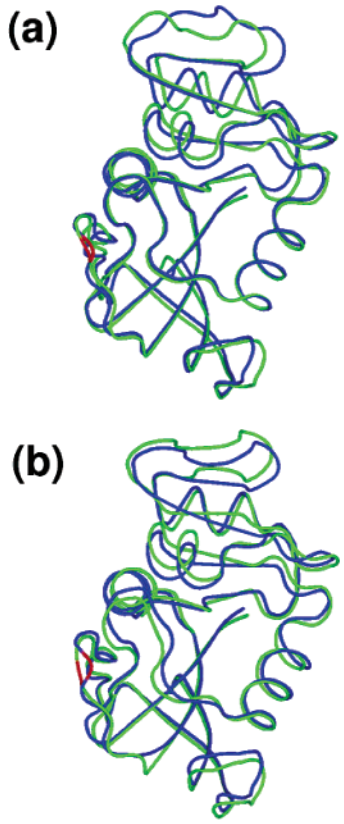

Figure 2. Average structures for wild-type (blue) and mutant (green) DHFR. The backbone structures are shown for (a) the reactant minimum and (b) the transition state of the free energy profile. The site of the mutation (residue 121) is shown in red for all structures. The average structures were generated as described in the text, and the figures were generated using the SwissPDB viewer[20] and the Pymol molecular graphics system.[41]

residue 121 is bulkier in the mutant enzyme than in the wild-type enzyme, the mutation does not appear to introduce adverse steric effects with residue 13. The simulations suggest that Val-121 has enough mobility to avoid steric clashes with other residues.

In addition to performing this structural analysis, we investigated the thermally averaged motions along the collective reaction coordinate. Figure 4 presents a comparison of representative thermally averaged motions for wild-type and mutant DHFR. Figure 4a shows that the donor−acceptor distance decreases as the reaction evolves from the reactant to the transition state for both enzymes. Table 1 shows that the average donor−acceptor distance at the transition state is 2.74 Å for both enzymes. Figure 4b shows that the angle between the acceptor carbon and methylene amino linkage in DHF increases as the reaction evolves from the reactant to the transition state for both enzymes, but the average angle at the transition state is slightly smaller for the mutant than for the wild-type enzyme.

Figure 4 also illustrates more dramatic differences in the motions of the wild-type and mutant enzymes. Figure 4c shows that the distance between C_ξ of Phe-31 and C11 of DHF decreases by ~1 Å as the reaction evolves from the reactant to the transition state for the wild-type enzyme but not for the mutant enzyme. For the wild-type enzyme, the motion of the Phe-31 toward the substrate may assist in directing the acceptor toward the donor as well as the opening of the angle between the acceptor carbon and the methylene amino linkage in DHF. Phe-31 is tightly conserved, and mutations of this residue have

(39) Hammes-Schiffer, S.; Tully, J. C. *J. Chem. Phys.* **1995**, *103*, 8528−8537.

Table 1. Average Distances and Angles in the Reactant and Transition States for the Wild-Type and G121V Mutant DHFR

	C_D–C_A	DHF tail ∠	Phe31–DHF	Asp122–Gly15	Ile14-NADPH
wild type (R)	3.31 (0.11)	113.97 (0.25)	6.03 (0.01)	2.97 (0.01)	2.87 (0.01)
wild type (TS)	2.74 (0.01)	116.44 (0.42)	4.91 (0.09)	3.38 (0.04)	2.97 (0.01)
G121V (R)	3.33 (0.11)	114.47 (0.17)	5.94 (0.05)	3.02 (0.01)	3.00 (0.01)
G121V (TS)	2.74 (0.01)	115.69 (0.54)	6.23 (0.01)	3.11 (0.02)	2.98 (0.01)

[a] R represents the reactant and TS represents the transition state. [b] Distances are in Angstroms and angles are in degrees. [c] Standard deviations are given in parentheses.

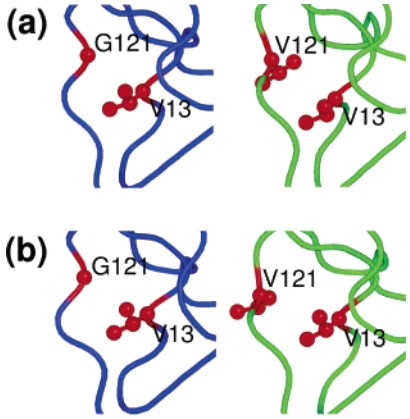

Figure 3. Average structures for wild-type (blue) and mutant (green) DHFR. The backbone structures are shown for (a) the reactant minimum and (b) the transition state of the free energy profile. Only the region of the enzyme near the mutated residue is shown, and the carbon atoms for residues 121 and 13 are shown explicitly in red. The average structures were generated as described in the text, and the figures were generated using the SwissPDB viewer[20] and the Pymol molecular graphics system.[41]

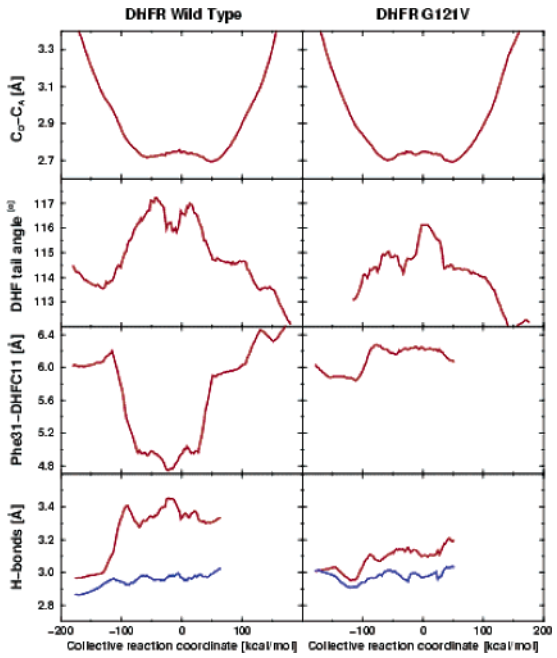

Figure 4. Equilibrium averages of geometrical properties along the collective reaction coordinate for wild-type (left) and mutant (right) DHFR: (a) donor−acceptor distance; (b) angle between the acceptor and methylene amino linkage in DHF; (c) distance between C_ζ of Phe-31 and C11 of DHF; (d) hydrogen-bonding distance between N of Asp-122 and O of Gly-15 (red) and between O of Ile-14 and carboxamide N of NADPH (blue).

been found to significantly decrease the rate of hydride transfer.[40,41] Figure 4d shows that the hydrogen bond between Asp-122 and Gly-15 increases by ∼0.4 Å as the reaction evolves from the reactant to the transition state for the wild-type but not for the mutant enzyme. (Note that hydrogen bonding motions are susceptible to difficulties with metastable states.) For both enzymes, the hydrogen bond distance between the Ile-14 and the NADPH coenzyme is nearly constant. For the wild-type enzyme, the motion of Gly-15 away from Asp-122, in conjunction with the constant hydrogen bond between Ile-14 and NADPH, may assist in directing the donor toward the acceptor. The absence of the motion of Phe-31 toward the substrate and the motion of Gly-15 away from Asp-122 in the mutant suggests that the mutation of Gly-121 may interrupt a network of coupled promoting motions.

In addition to these equilibrium simulations, we performed dynamical calculations of the transmission coefficients using the MDQT reactive flux method. The transmission coefficient was determined to be 0.89 for the wild-type enzyme and 0.80 for the mutant enzyme. Because the estimated uncertainty in these values is ±0.05, the difference between these values is not statistically significant. Moreover, this difference would not account for a substantial change in the rate because the transmission coefficient is a prefactor in the rate expression given in eq 4. Thus, these calculations show that the decrease in the hydride transfer rate for the G121V mutant is due to an increase in the free energy barrier.

IV. Discussion and Conclusions

This paper presents hybrid quantum-classical simulations of the G121V mutant DHFR. Although this mutation is on the exterior of the enzyme and is more than 12 Å from the transferring hydride, experiments indicate a rate reduction by a factor of 163. All aspects of the mutant calculations were the same as previous wild-type DHFR calculations except for the replacement of Gly-121 with valine. The calculated free energy barrier is 3.4 kcal/mol higher for the G121V mutant than for the wild-type DHFR. This result is qualitatively consistent with the experimentally observed rate reduction, which corresponds to an increase in the free energy barrier of 3.0 kcal/mol (neglecting barrier recrossing effects). The calculated transmission coefficients are comparable for the wild-type and mutant enzymes. These results indicate that the decrease in the rate for the G121V mutant is due to an increase in the free energy barrier rather than a decrease in the transmission coefficient. In general, changes to the free energy barrier have a greater effect on the rate than changes to the transmission coefficient because the free energy is in the exponent, whereas the transmission coefficient is a prefactor in the rate expression.

The simulations suggest that the increase in the free energy barrier may arise from the interruption of a network of coupled promoting motions in DHFR.[6] Here, promoting motions are

(40) Chen, J. T.; Taira, K.; Tu, C. P. D.; Benkovic, S. J. *Biochemistry* **1987**, *26*, 4093−4100.

(41) DeLano, W. L.; DeLano Scientific: San Carlos, California, 2002.

defined as systematic changes in thermally averaged properties as the reaction evolves along the collective reaction coordinate. They represent the conformational changes that occur during the reaction and correspond to the reorganization of the environment for the charge-transfer process. These motions occur on the time scale of the hydride transfer reaction, which has been experimentally determined to be on the millisecond time scale for DHFR.[23] Some of the promoting motions observed in the wild-type DHFR were found to be diminished or absent in the mutant enzyme. In particular, the distance between Phe-31 and the substrate decreases and the hydrogen bond between Asp-121 and Gly-15 increases as the reaction evolves from the reactant to the transition state for the wild-type DHFR. These motions are not observed in the G121V mutant enzyme.

These results suggest that a mutation on the exterior of an enzyme can interrupt a network of coupled promoting motions and thereby significantly decrease the reaction rate. This phenomenon has broad implications for protein engineering and drug design. Additional studies are required to test this hypothesis and to further elucidate the role of motion in enzyme catalysis.

Acknowledgment. We thank Steve Benkovic, Ravi Rajogopalan, Salomon Billeter, and Kim Wong for helpful discussions. We are grateful for financial support from National Institutes of Health Grant GM56207.

JA028487U